Supporting Information

Facile Mass Production of Self-Supported Two-Dimensional Transitional Metal Oxides for Catalytical Applications

Yihong Kang, [a] *Hanhan Xie,* [a] *Danni Liu,*[a] *Ming Gao,* [a] *Paul K Chu,* [b] *Seeram Ramakrishna,* [c] *and Xue-Feng Yu*[a,]*

[a] Material Interfaces Center, Shenzhen Institutes of Advanced Technology, Chinese Academy of Sciences, Shenzhen 518055, China.

[b] Department of Physics and Department of Materials Science and Engineering, City University of Hong Kong, Tat Chee Avenue, Kowloon, Hong Kong, China

[c] Department of Mechanical Engineering, National University of Singapore, 9 Engineering Drive 1, Singapore 117576

Email: xf.yu@siat.ac.cn

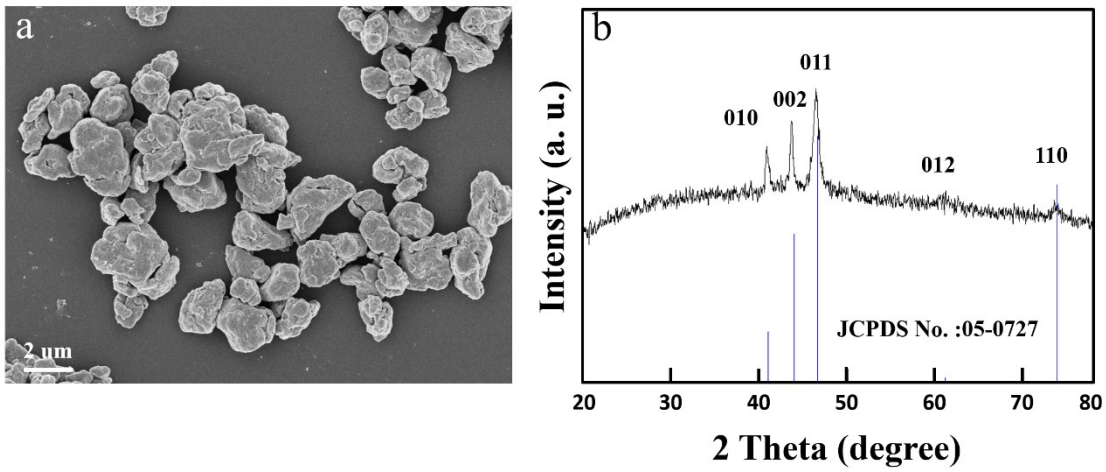

Figure S1. (a) SEM image and (b) XRD spectra of the original cobalt powder.

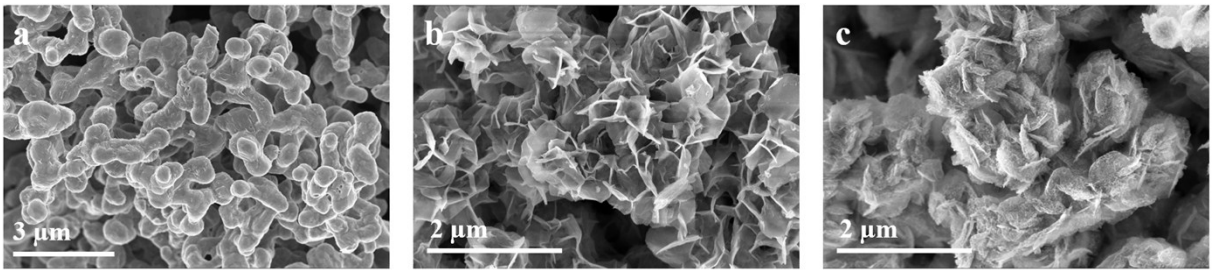

Figure S2. (a) SEM image of cobalt powders after immersing in H_2SO_4 solution (pH=2) for 48 hours, showing the lack of self-supported 2D structure formation; (b) SEM image of cobalt powders after immersing in $FeSO_4$ solution (2mg/ml) for 48 hours, showing the formation of self-supported 2D structure; (c) SEM image of cobalt powders after immersing in NaOH solution (pH=13) for 48 hours, showing the formation of self-supported 2D structure with denser nanosheets and more tiny nuclei on the nanosheets.

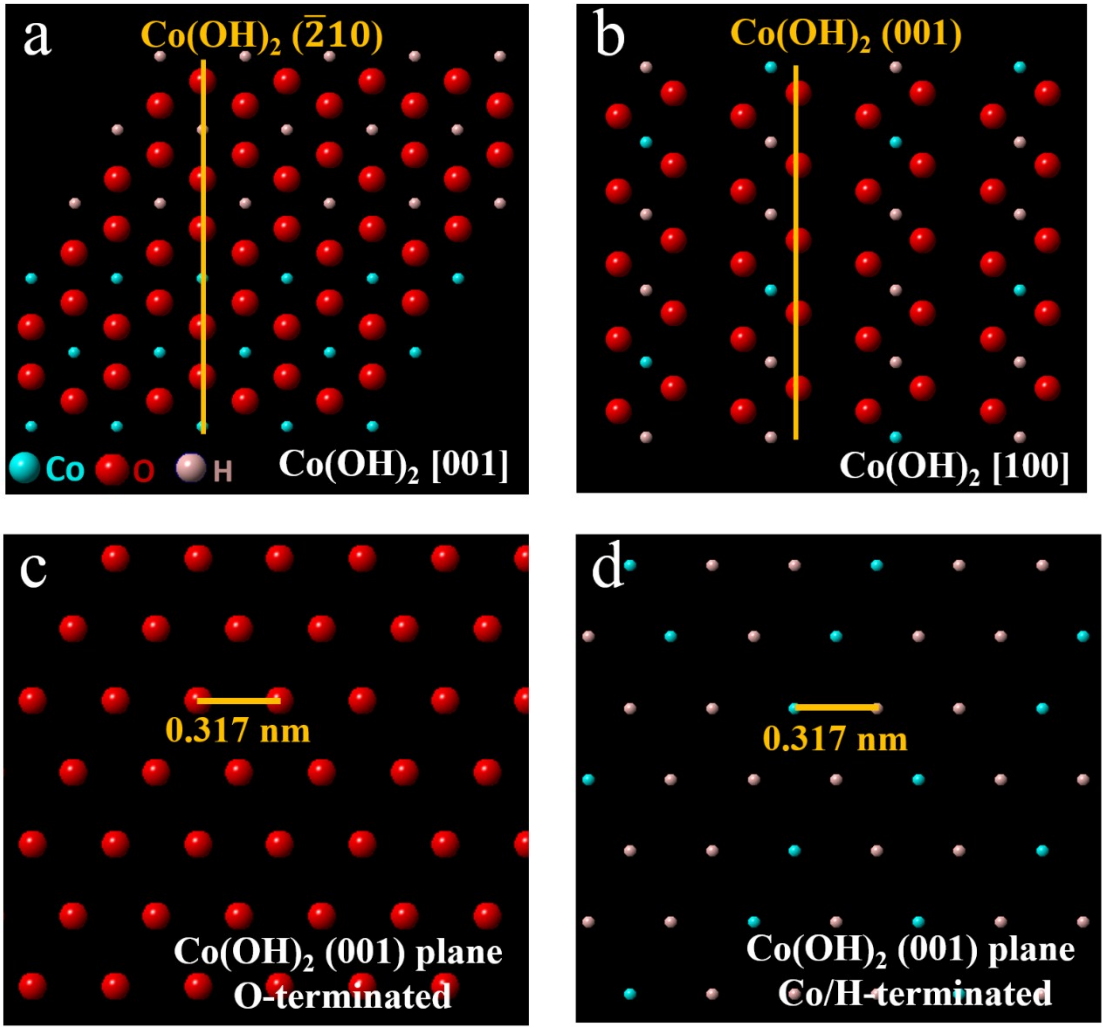

Figure S3. Simulated crystal structure of $Co(OH)_2$: (a) Crystal structure of $Co(OH)_2$ along the [001] zone axis; (b) Crystal structure of $Co(OH)_2$ along the [100] zone axis; (c) Atomic arrangement of the O-terminated $Co(OH)_2$ (001) plane; (d) Atomic arrangement of the Co/H-terminated $Co(OH)_2$ (001) plane. Co and H have the same occupation of space and therefore, the distribution displayed in the simulation is randomly arranged according to the stoichiometric ratio.

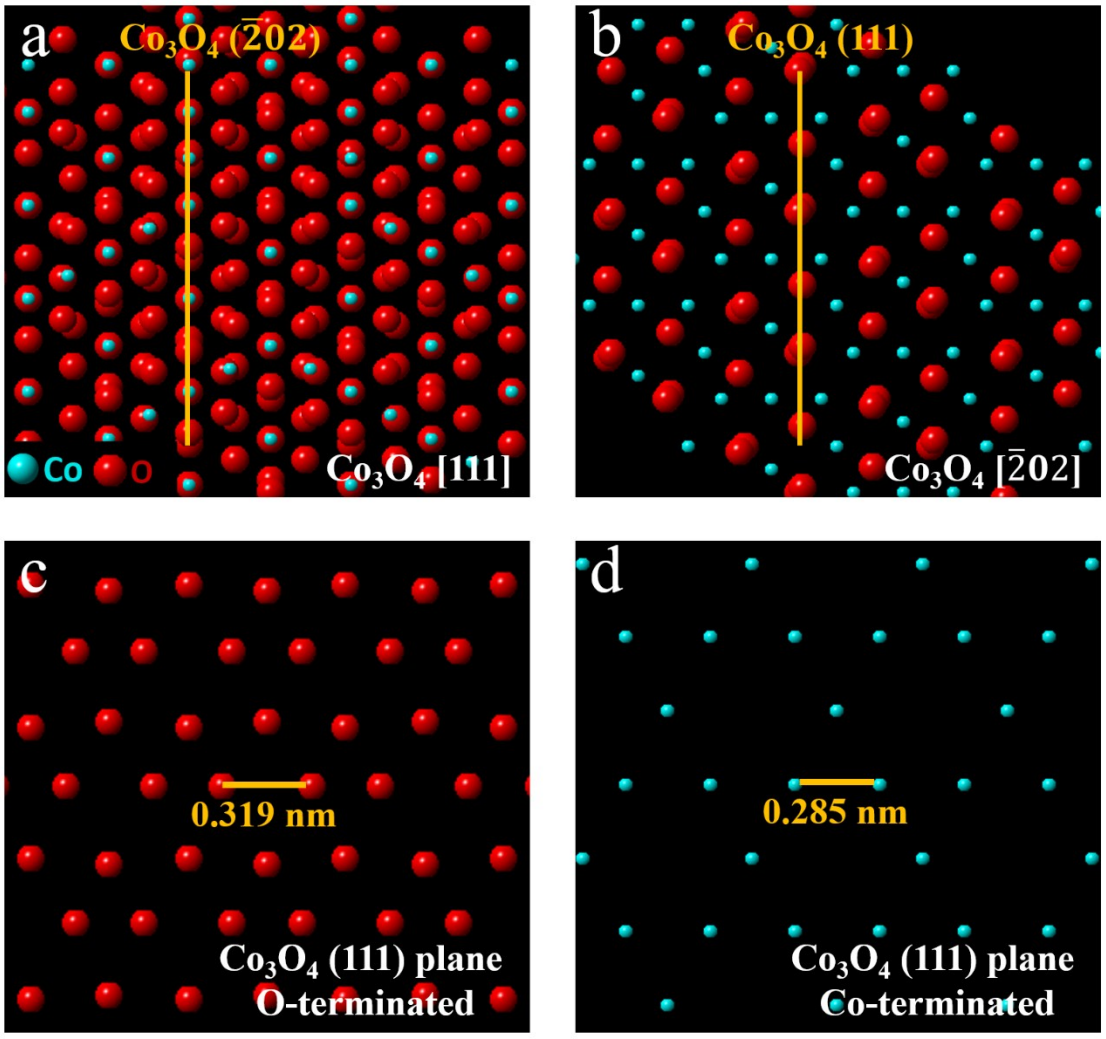

Figure S4. Simulated crystal structure of Co_3O_4: (a) Crystal structure of Co_3O_4 along the [111] zone axis; (b) Crystal structure of Co_3O_4 along the [$\bar{2}02$] zone axis; (c) Atomic arrangement of the O-terminated Co_3O_4 (111) plane; (d) Atomic arrangement of the Co-terminated Co_3O_4 (111) plane.

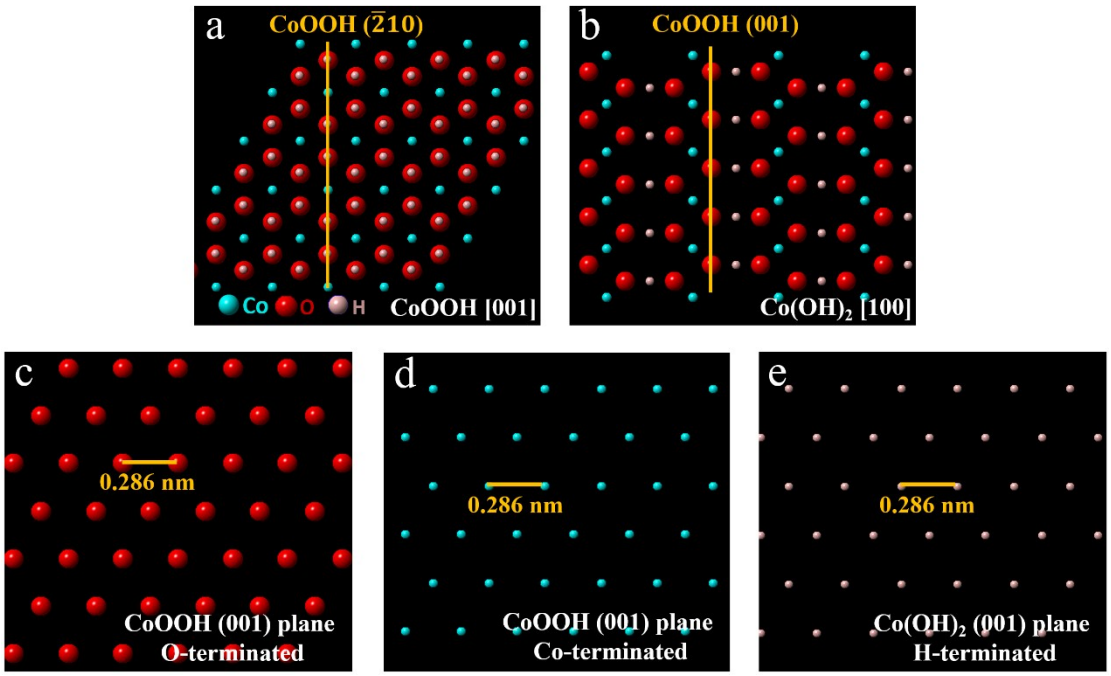

Figure S5. Simulated crystal structure of CoOOH: (a) Crystal structure of CoOOH along the [001] zone axis; (b) Crystal structure of CoOOH along the [100] zone axis; (c) Atomic arrangement of the O-terminated CoOOH (001) plane; (d) Atomic arrangement of the Co-terminated CoOOH (001) plane; (e) Atomic arrangement of the H-terminated CoOOH (001) plane.

In the basic solution, $Co(OH)_2$ is converted into the thermodynamically more stable CoOOH. Although CoOOH has a similar (001) plane configuration as $Co(OH)_2$, it possesses a smaller lattice constant and different crystal symmetry. Hence, when CoOOH grows epitaxially on $Co(OH)_2$, there is a 10% lattice mismatch. Moreover, Co in CoOOH exists as Co^{3+}, which is significantly more difficult to produce in an aqueous solution than Co^{2+}.[1] Consequently, the amount of CoOOH formed during the corrosion process is limited as indicated by the weak diffraction pattern (Figure 3e). The following equation shows the chemical reaction for the transformation from $Co(OH)_2$ to CoOOH in the basic solution:

$$Co(OH)_2 + OH^- \rightarrow CoOOH + H_2O + e^-.$$

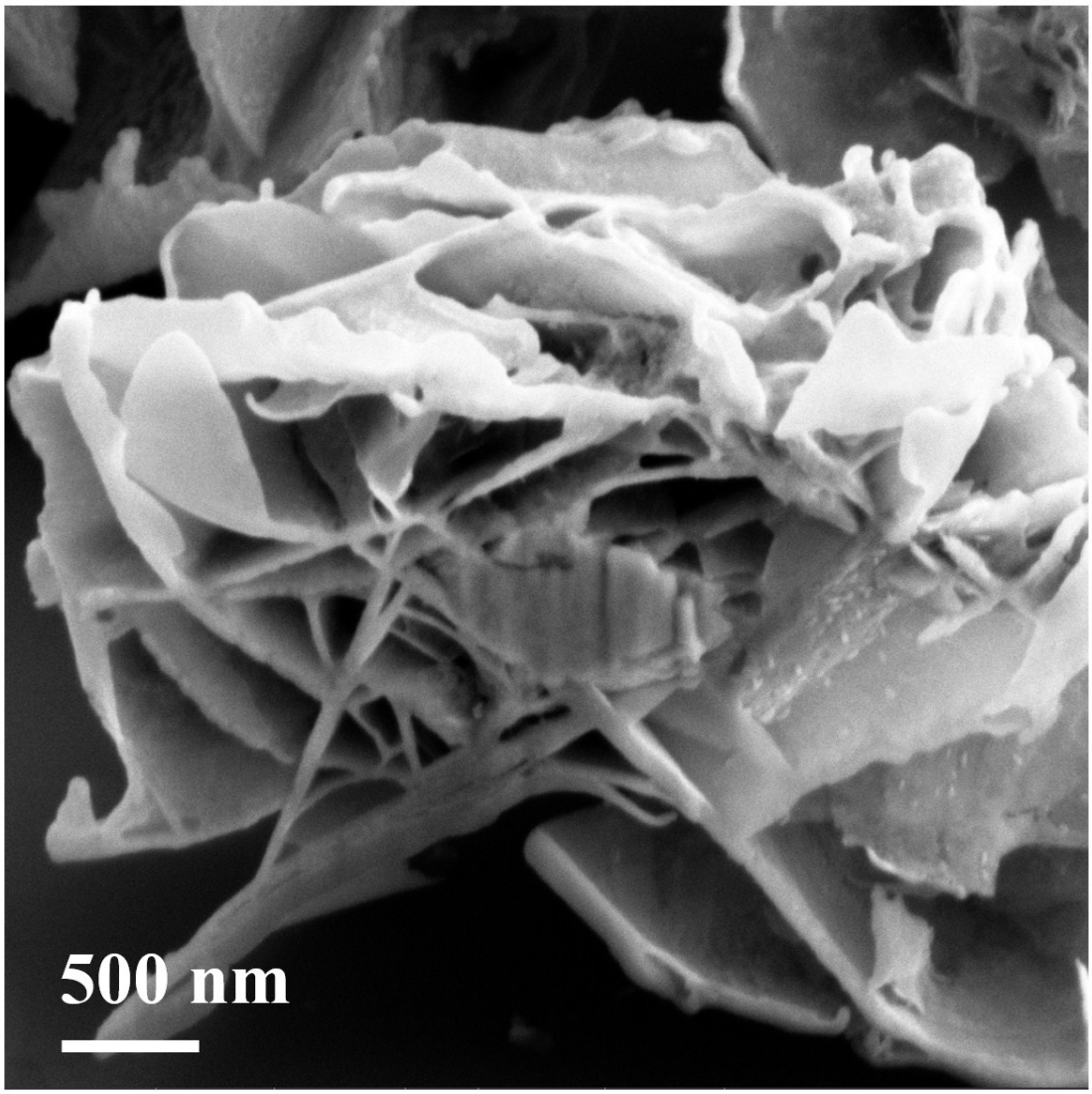

Figure S6. Cross-sectional view of the representative self-supported 2D Co_3O_4.

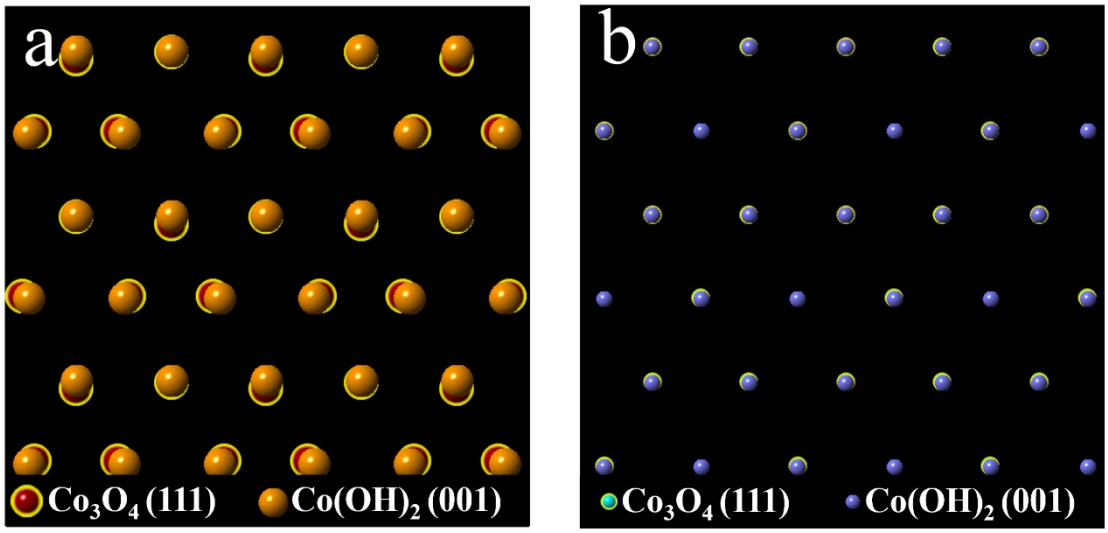

Figure S7. Simulated atomic arrangement of CoOOH (001) grown epitaxially on Co_3O_4 (111): (a) O-terminated plane and (b) Co-terminated plane.

During the OER process, oxyhydroxides may form as intermediate products.[2] Since the 2D Co_3O_4 has a preferential (111) orientation, which has a good epitaxial relationship with CoOOH (001) (Co_3O_4 ($\bar{4}04$) // CoOOH ($\bar{2}10$) and Co_3O_4 (111) // CoOOH (001)), on-site transformation from Co_3O_4 to CoOOH is achieved without introducing an excessive amount of stress. This low-stress on-site transformation preserves the 2D morphology during the OER process giving rise to excellent stability.

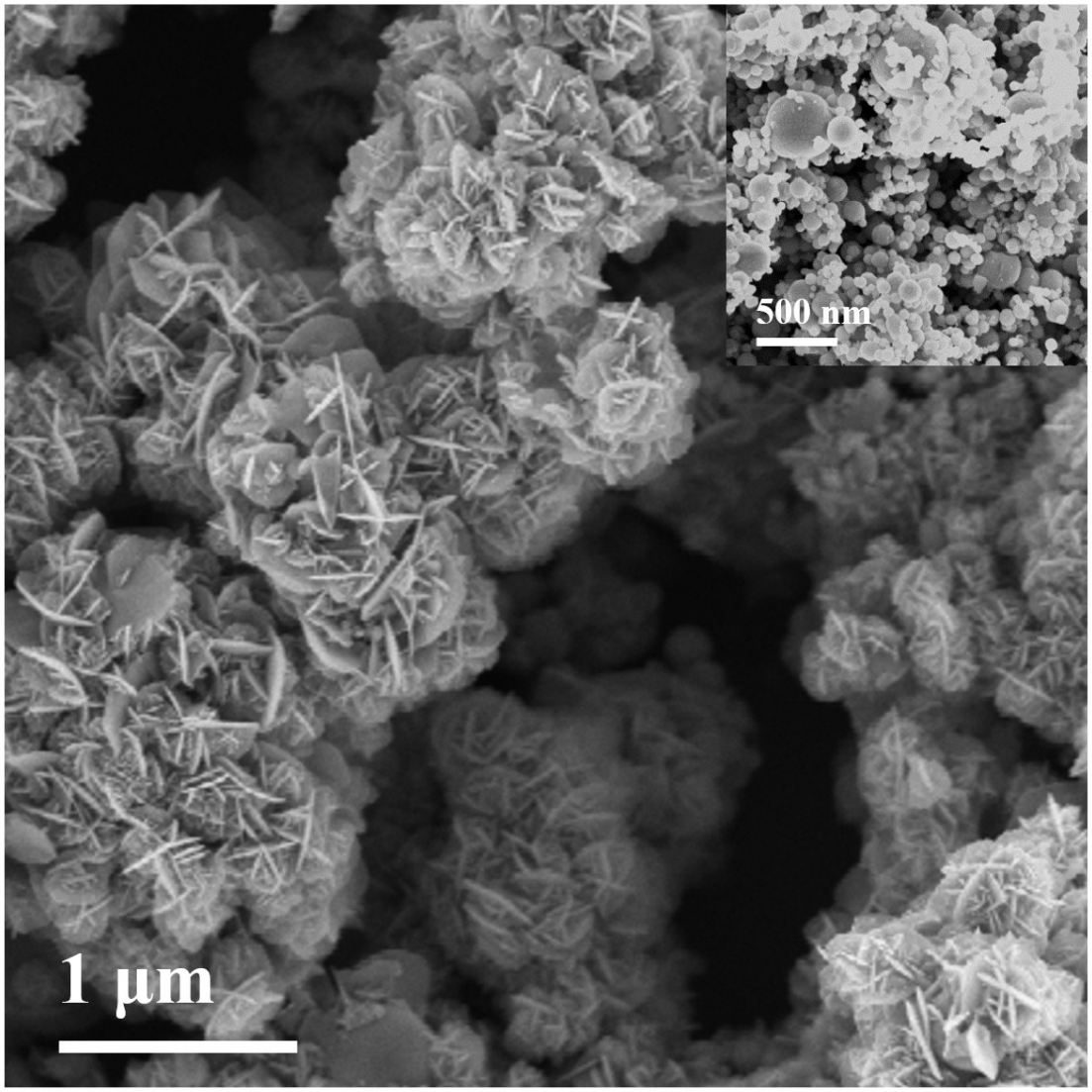

Figure S8. SEM image of the self-supported 2D Co_3O_4 produced by corrosion of nano-size (about 100 nm) cobalt powders in 24 hours with the inset showing the SEM image of the original cobalt powders.

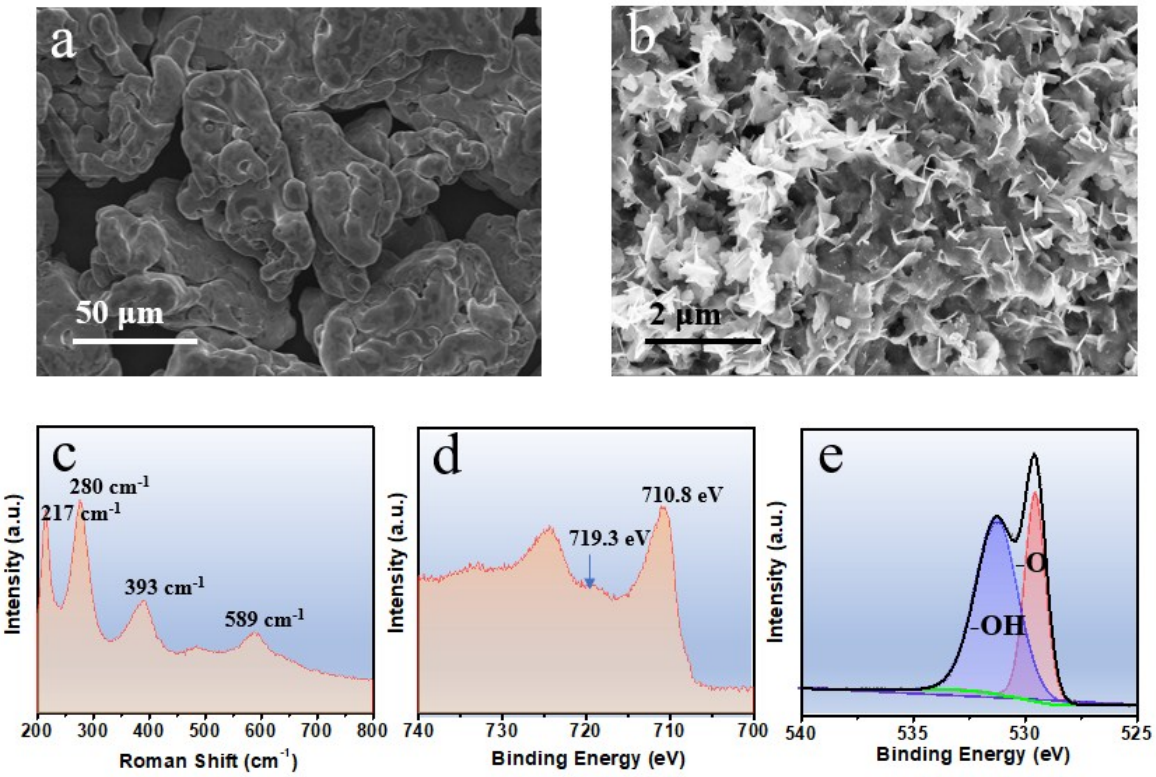

Figure S9. Structure and phase analysis of the self-supported 2D Fe_2O_3 formed by immersing in water for 24 hours at 50℃. (a) SEM image of Fe powder. (b) SEM image of self-supported 2D Fe_2O_3. (c) Raman scattering spectrum. (d) XPS spectrum of Fe 2p. (e) XPS spectrum of O 1s.

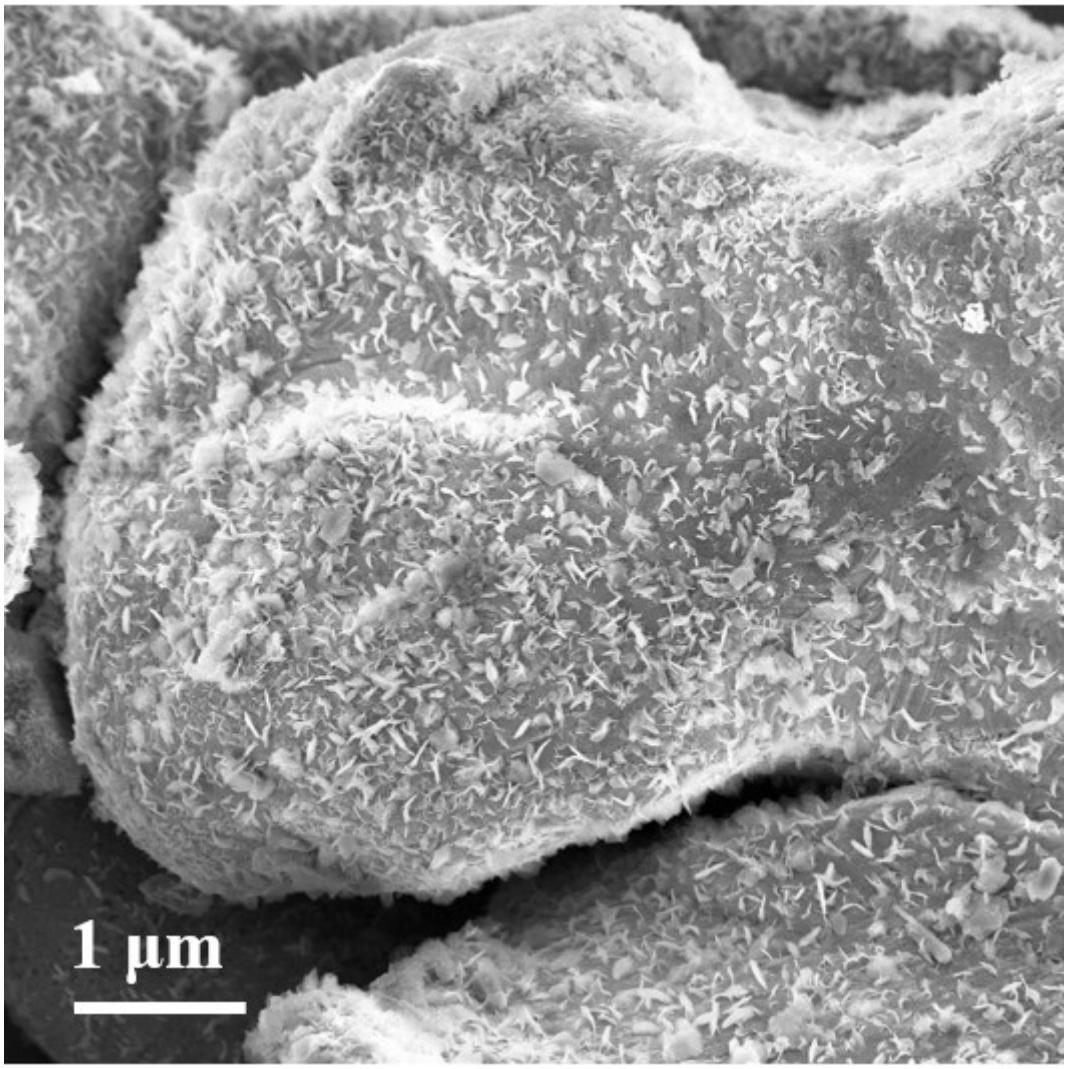

Figure S10. SEM image of the Fe_2O_3 nanosheets formed on the Fe particles after immersing in water for 48-hour at room temperature.

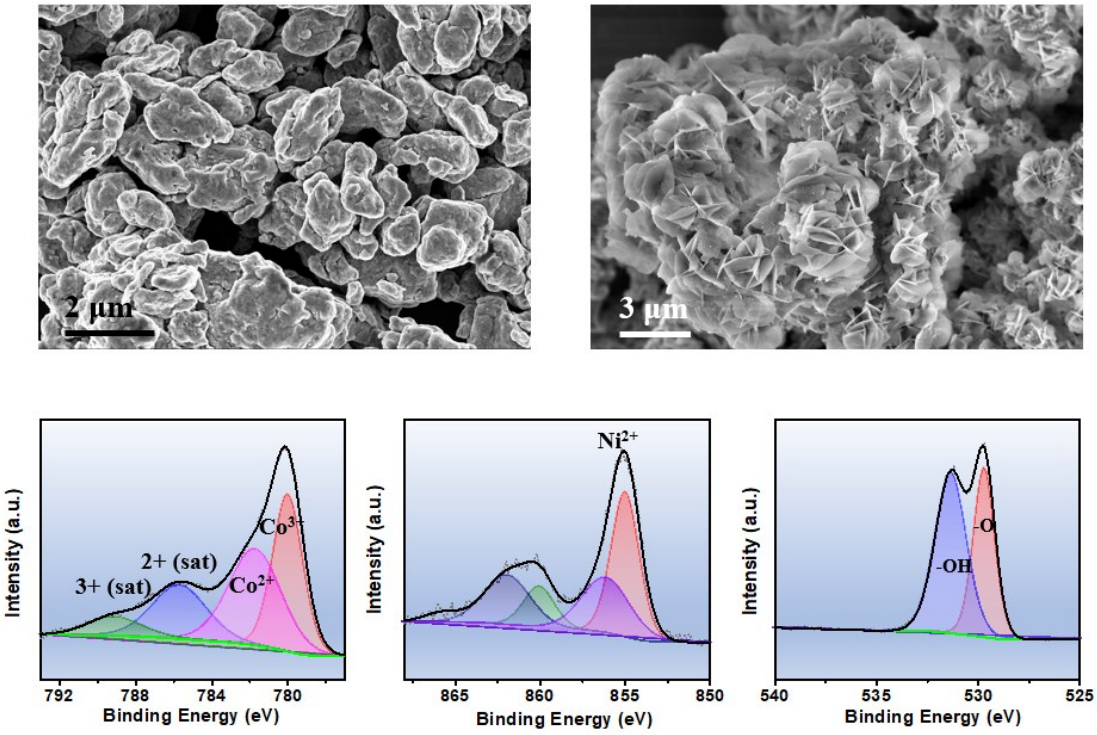

Figure S11. (a) SEM image of original NiCo alloy powders. (b) SEM image of the self-supported 2D $Ni_xCo_{3-x}O_4$ after immersing NiCo powders in water for 24-hour at 50 ˚C. XPS analysis of (c) Co 2p, (d) Ni 2p and (e) O 1s.

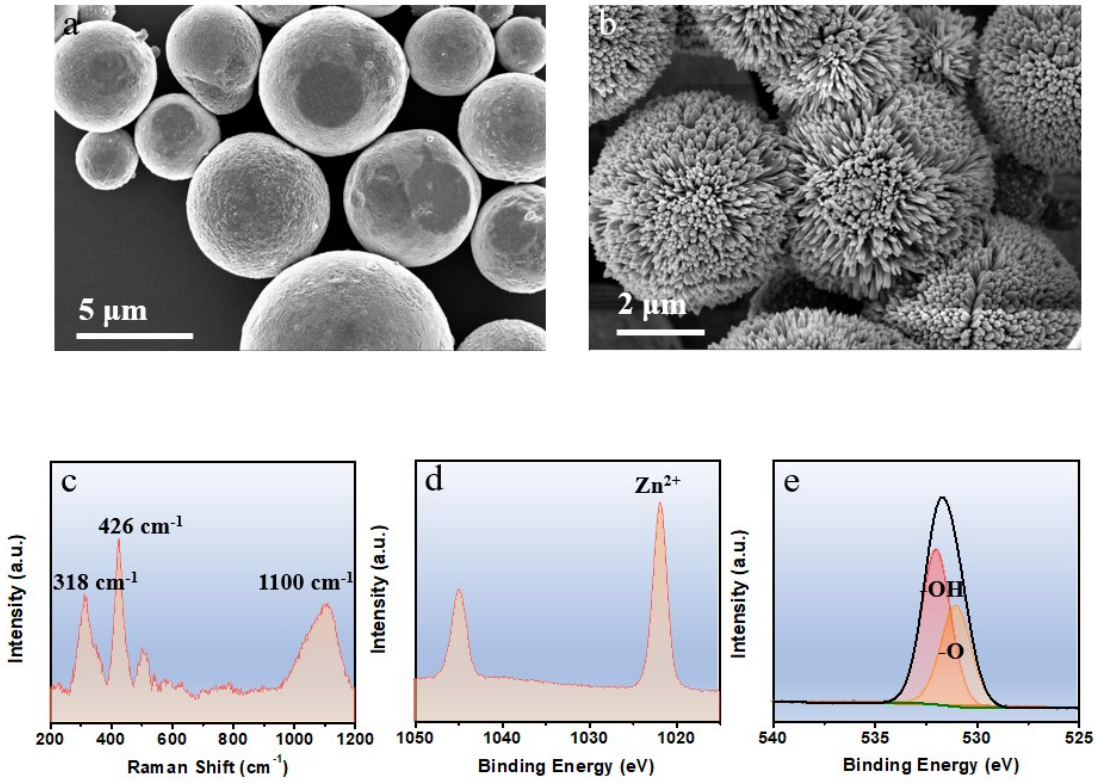

Figure S12. (a) SEM image of original Zn powders. (b) SEM image of the self-supported ZnO nanorods after immersing Zn powders in water for 12-hour at 70 ˚C. (c) Raman scattering spectrum of the products. XPS analysis of (d) Zn 2p and (e) O 1s.

Table S1. Production details of self supported 2D Co_3O_4.

Product	Reaction temperature (˚C)	Reaction time (hour)	Solvent	Weight of solvent (kg/run)	Weight of the metal powders (g/run)	Size of the metal powders (μm)	Average Yield (g/run)	Runs of experiments	Total Yield (g)
Self-supported 2D Co_3O_4	28	48	Water	2	200	2	223	4	870
Self-supported 2D Fe_2O_3	28	48	Water	1	100	50	100	1	100
Self-supported 2D Fe_2O_3	50	24	Water	1	100	50	110	1	110
Self-supported 2D $Ni_xCo_{3-x}O_4$	50	24	Water	1	100	2	115	1	115

Table S2. Comparison of the water oxidation performance of catalysts.

Catalyst	Onset potential (V *vs.* RHE)	Tafel slope (mV dec^{-1})	Potential@100mA cm^{-2} (V *vs.* RHE)	Potential@300mA cm^{-2} (V *vs.* RHE)	Electrolyte	Substrate	Reference
Self-supported 2D Co_3O_4	1.50	62	1.61	1.65	1 M KOH	Carbon cloth	This work
Co_3O_4-MTA	1.51	84	1.58	1.65	1 M KOH	Ni foam	3
$Co_3O_4/NiCo_2O_4$ nanocages	1.53	88	1.72	N.A.	1 M KOH	Ni foam	4
Reduced Mesoporous Co_3O_4 nanowires	1.52	72	N.A.	N.A.	1 M KOH	Glassy carbon	5
Carbon-coated Co_3O_4 nanoarrays	1.54	82	1.69	N.A.	0.5 M H_2SO_4	Carbon paper	6
NiFe-LDH nanoplatelet arrays	1.43	52.8	1.63	1.68	1 M KOH	Ni foam	7
Black phosphorus/Co_2P nanosheets	1.55	78	1.72	N.A.	1 M KOH	Glassy carbon	8
Carbo- coated porous Ni_2P nanoplates	1.48	64	N.A.	N.A.	1 M KOH	Glassy carbon	9
Ni_3Se_2–Ni foam	1.46	142.8	1.83	N.A.	0.3 M KOH	Ni foam	10
Delithiated $LiCoO_2$	1.52	50	N.A.	N.A.	0.1 M KOH	Carbon paper	11

References

1 D. R. Lide, ed., *CRC Handbook of Chemistry and Physics*, Taylor & Francis, Boca Raton, Florida, 2006.
2 E. Fabbri, M. Nachtegaal, T. Binninger, X. Cheng, B.-J. Kim, J. Durst, F. Bozza, T. Graule, R. Schaublin, L. Wiles, M. Pertoso, N. Danilovic, K. E. Ayers and T. J. Schmidt, *Nat Mater*, 2017, **16**, 925-931.
3 Y. P. Zhu, T. Y. Ma, M. Jaroniec and S. Z. Qiao, *Angew*
. *Chemie. Int. Ed.*, 2017, **56**, 1324-1328.
4 H. Hu, B. Guan, B. Xia and X. W. Lou, *J. Amer. Chem. Soc.*, 2015, **137**, 5590-5595.
5 Y. Wang, T. Zhou, K. Jiang, P. Da, Z. Peng, J. Tang, B. Kong, W.-B. Cai, Z. Yang and G. Zheng, *Adv. Energy Mater.*, 2014, **4**, 1400696-n/a.
6 X. Yang, H. Li, A.-Y. Lu, S. Min, Z. Idriss, M. N. Hedhili, K.-W. Huang, H. Idriss and L.-J. Li, *Nano Energy*, 2016, **25**, 42-50.
7 Z. Li, M. Shao, H. An, Z. Wang, S. Xu, M. Wei, D. G. Evans and X. Duan, *Chemical Science*, 2015, **6**, 6624-6631.
8 J. Wang, D. Liu, H. Huang, N. Yang, B. Yu, M. Wen, X. Wang, P. K. Chu and X. F. Yu, *Angew. Chem.*, 2018, **130**, 2630-2634.
9 X.-Y. Yu, Y. Feng, B. Guan, X. W. Lou and U. Paik, *Energy & Environ. Sci.*, 2016, **9**, 1246-1250.
10 A. T. Swesi, J. Masud and M. Nath, *Energy & Environ. Sci.*, 2016, **9**, 1771-1782.
11 Z. Lu, H. Wang, D. Kong, K. Yan, P.-C. Hsu, G. Zheng, H. Yao, Z. Liang, X. Sun and Y. Cui, *Nat. Commun.*, 2014, **5**, 4345.